

# Bold Diagrammatic Monte Carlo Method Applied to Fermionized Frustrated Spins

S. A. Kulagin<sup>1,2</sup>, N. Prokof'ev<sup>1,3</sup>, O. A. Starykh<sup>4</sup>, B. Svistunov<sup>1,3</sup>, and C. N. Varney<sup>1</sup>

<sup>1</sup>*Department of Physics, University of Massachusetts, Amherst, Massachusetts 01003, USA*

<sup>2</sup>*Institute for Nuclear Research of Russian Academy of Sciences, 117312 Moscow, Russia*

<sup>3</sup>*Russian Research Center "Kurchatov Institute", 123182 Moscow, Russia*

<sup>4</sup>*Department of Physics and Astronomy, University of Utah, Salt Lake City, Utah 84112, USA*

(Dated: October 30, 2018)

We demonstrate, by considering the triangular lattice spin-1/2 Heisenberg model, that Monte Carlo sampling of skeleton Feynman diagrams within the fermionization framework offers a universal first-principles tool for strongly correlated lattice quantum systems. We observe the fermionic sign blessing—cancellation of higher order diagrams leading to a finite convergence radius of the series. We calculate the magnetic susceptibility of the triangular-lattice quantum antiferromagnet in the correlated paramagnet regime and reveal a surprisingly accurate microscopic correspondence with its classical counterpart at all accessible temperatures. The extrapolation of the observed relation to zero temperature suggests the absence of the magnetic order in the ground state. We critically examine the implications of this unusual scenario.

PACS numbers: 02.70.Ss, 05.10.Ln

The method of bold diagrammatic Monte Carlo simulation (BDMC) [1] allows one to sample contributions from millions of skeleton Feynman diagrams and extrapolate the results to the infinite diagram order, provided the series is convergent (or subject to resummation beyond the convergence radius). Recent experimentally certified application of BDMC to unitary fermions down to the point of the superfluid transition [2] makes a strong case for BDMC method as a generic method for dealing with correlated fermions described by Hamiltonians without small parameters. One intriguing avenue to explore is to apply it to frustrated lattice spin systems, where, on one hand, standard Monte Carlo (MC) simulation fails because of the sign problem [3], and, on the other hand, the system's Hamiltonian can be always written in the fermionic representation [4–6] which contains no large parameters—exactly what is needed for the anticipated convergence of BDMC series with the diagram order.

The BDMC approach is based on the *sign blessing* phenomenon, when, despite the factorial increase in the number of diagrams with expansion order, the series features a finite convergence radius because of dramatic (sign alternation induced) compensation between the diagrams. With the finite convergence radius, the series can be summed either directly, or with resummation techniques that can be potentially applied down to the critical temperature of the phase transition, if any. (At the critical temperature thermodynamic functions become nonanalytic, and the diagrammatic expansion involving explicit symmetry breaking by the finite order parameter is necessary to treat the critical region and the phase with broken symmetry.) In the absence of the sign blessing, the resummation protocols become questionable in view of the known mathematical theorems regarding asymptotic series. At the moment, there is no theory allowing one to prove the existence of a finite convergence radius analytically. The absence of Dyson's

collapse [7] in a given fermionic system is merely providing hope that the corresponding diagrammatic series is not asymptotic and cannot be *a priori* taken as a sufficient condition for the sign blessing. Hence, the applicability of BDMC method to a given system can be established only on the basis of a direct numerical evidence for series convergence and comparison with either experiment or alternative controllable techniques, such as high-temperature series [8] and numerical linked cluster (NLC) expansions [9]. In this Letter, we report the first successful application of BDMC method to fermionized quantum spin systems by simulating the canonical model of frustrated quantum magnetism—the triangular lattice antiferromagnetic spin-1/2 Heisenberg model (TLHA). We demonstrate that BDMC method for this frustrated magnet *is indeed* subject to the sign blessing phenomenon which allows us to obtain basic static and dynamic correlation functions with controllable (about one percent or better) accuracy. The agreement with extrapolated high-temperature expansions is excellent.

In addition, we report a very surprising finding of extreme similarity between short-distance static spin correlations of the quantum and classical spin models, evaluated at different but uniquely related to each other temperatures. This accurate (within the error bars) quantum-to-classical correspondence holds at all temperatures accessible to us,  $T \geq 0.375$  (here and below temperature is measured in the units of the exchange constant  $J$ ). Specifically, the *entire* static correlation function of the quantum model at a given temperature  $T$ —having quite nontrivial pattern of sign-alternating spatial dependence and temperature evolution, thus forming a system's fingerprint—turns out to be equal, up to a global temperature dependent normalization factor, to its classical counterpart at a certain temperature  $T_{cl} \equiv T_{cl}(T)$ . Extrapolation of the obtained  $T_{cl}(T)$  curve to the  $T = 0$  limit results in a finite value of  $T_{cl}(0) > 0$ ,

suggesting a quantum-disordered ground state of the quantum model.

The Hamiltonian of the TLHA is given by

$$H = J \sum_{\langle i,j \rangle} \vec{S}_i \cdot \vec{S}_j. \quad (1)$$

Here  $\vec{S}_i$  is the spin-1/2 operator on the  $i$ th site of the triangular lattice and the sum is over the nearest neighbor pairs coupled by the positive exchange integral,  $J > 0$ . As found by Popov and Fedotov [4, 5], the grand canonical Gibbs distribution of the model (1) can be reformulated identically in terms of purely fermionic operators using

$$\vec{S}_i = \frac{1}{2} \sum_{\alpha,\beta} f_{i\alpha}^\dagger \vec{\sigma}_{\alpha\beta} f_{i\beta}, \quad (2)$$

where  $f_{i\beta}$  is the second quantized operator annihilating a fermion with spin projection  $\alpha, \beta = \pm 1$  on site  $i$ , and  $\vec{\sigma}$  are the Pauli matrices. The representation (2) leads to a flat-band fermionic Hamiltonian,  $H_F$ , with two-body interactions and amenable to direct diagrammatic treatment. To eliminate statistical contributions from non-physical states having either zero or two fermions, Ref. 4 introduced an imaginary chemical potential to  $H_F$ :

$$H_F \rightarrow H_F - i(\pi/2)T \sum_i (n_i - 1), \quad n_i = \sum_\alpha f_{i\alpha}^\dagger f_{i\alpha}. \quad (3)$$

The added term commutes with the original Hamiltonian and has no effect on properties of the physical subspace  $\{n_i = 1\}$  whatsoever. Moreover, the grand canonical partition functions and spin-spin correlation functions of the original spin model and its fermionic version are also identical because (i) physical and nonphysical sites decouple in the trace and (ii) the trace over non-physical states yields identical zero on every site. As a result, one arrives at a rather standard Hamiltonian for fermions interacting through two-body terms. A complex value of the chemical potential, which can also be viewed as a peculiar shift of the fermionic Matsubara frequency  $\omega_n = 2\pi(n + 1/2)T \rightarrow 2\pi(n + 1/4)T$ , is a small price to pay for the luxury of having the diagrammatic technique.

We perform BDMC simulations using the standard  $G^2W$ -skeleton diagrammatic expansion of the fermionic model (1)-(3) in the real space-imaginary time representation [10], see also [11]. The first and most important question to answer is whether the sign blessing phenomenon indeed takes place. In Fig. 1 we show comparison between the calculated answer for the static uniform magnetic susceptibility,  $\chi_u$ , and the NLC expansion result [9] at  $T = 2$ . This temperature is low enough to ensure that we are in the regime of strong correlations because  $\chi_u$  is nearly a factor of two smaller than the free-spin answer  $\chi_u^{(0)} = 1/4T$ . On the other hand, this

temperature is high enough to be sure that the high-temperature series can be described by Padé approximants without significant systematic deviations from the exact answer [8, 9] (at slightly lower temperature the bare NLC series starts to diverge). We clearly see that the BDMC series converges to the correct result with an accuracy of about three meaningful digits and there is no statistically significant change when more than a hundred thousand of 7th order diagrams [12] are accounted for. The error bar for the 7th order point is significantly increased due to factorial growth in computational complexity. Feynman diagrams are usually formulated for the system in the thermodynamic limit. In practice, for reasons of convenient data handling, our code works with finite system sizes  $L$  with periodic boundary conditions (its performance does not depend on  $L$ ). In all cases we choose  $L$  to be much larger than the correlation length  $\xi$  and check that doubling the system size makes no detectable changes in the final answer. The 4th order result can be obtained after several hours of CPU time on a single processor.

Interestingly enough, when temperature is lowered down to  $T = 1$  which is significantly below the point where the bare NLC series start to diverge, see Fig. 2, the BDMC series continue to converge exponentially. This underlines the importance of performing simulations within the self-consistent skeleton formulation.

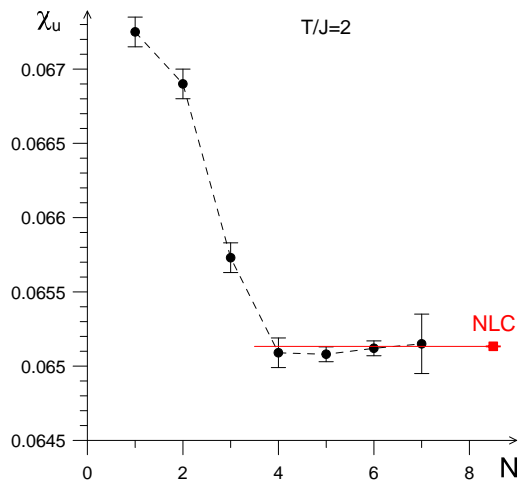


FIG. 1. (Color online) Uniform susceptibility calculated within the  $G^2W$ -skeleton expansion as a function of the maximum diagram order retained in the BDMC simulation (black dots) for  $T/J = 2$ . The result of the high-temperature expansion (with Padé approximant extrapolation) [8, 9] is shown by the red square and horizontal line.

In Fig. 2 we show results of the BDMC simulation performed at temperatures significantly below the mean-field transition temperature. We observe excellent agreement (within our error bars) with the Padé approximants used to extrapolate the high-temperature series

data to lower temperature [8]. Within the current protocol of dealing with skeleton diagrams we were not able to go to a lower temperature due to the development of near singularity in the response function (and thus in the effective-interaction propagator) at the classical ordering wave vector  $\mathbf{Q} = (4\pi/3, 0)$ , in units of inverse lattice constant. In future work, we plan to apply pole-regularization schemes to overcome this technical problem.

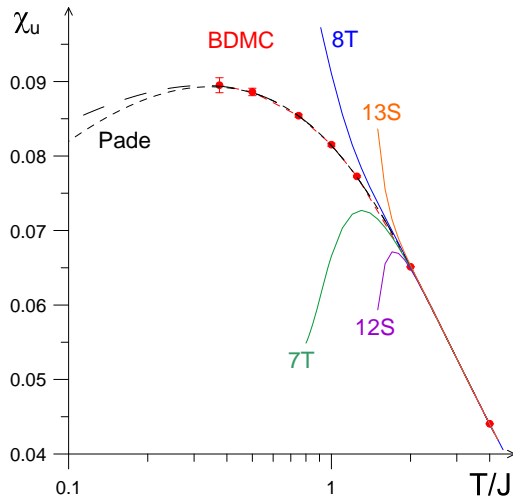


FIG. 2. (Color online) Uniform susceptibility as a function of temperature (red dots) for the triangular Heisenberg antiferromagnet calculated within the BDMC approach. NLC expansion results based on triangles (labeled as 7T and 8T) and sites (labeled as 12S and 13S) [9] are shown along with two different Padé approximant extrapolations [8].

We now turn to the static susceptibility

$$\chi(\mathbf{r}) = \int_0^{1/T} d\tau \langle S_{\mathbf{0}}^z(0) S_{\mathbf{r}}^z(\tau) \rangle. \quad (4)$$

Here  $S_{\mathbf{r}}^z(\tau)$  is the Matsubara spin operator on the lattice site labeled by the integer index vector  $\mathbf{r}$ . For the simplicity of comparing susceptibility (4) with its classical counterpart, we normalize it to unity at the origin,  $\chi(\mathbf{r}) \rightarrow \chi(\mathbf{r})/\chi(\mathbf{0})$ , doing the same with the classical  $\chi_{\text{cl}}(\mathbf{r})$ . The latter is obtained by Metropolis simulation of the classical Heisenberg model (1) in which quantum spin operators are replaced with classical unit vectors  $\mathbf{n}_{\mathbf{r}}$ . For every accessible temperature  $T$  we observe a perfect match (within the error bars, which are about 1%) between quantum correlator  $\chi(\mathbf{r})$  and its classical counterpart, for  $r$  ranging from 1 to 5 (which includes 10 different sites), calculated at a certain temperature  $T_{\text{cl}}(T)$ . A typical example of the match is presented in Fig. 3. We note in passing that the equal-time correlation function,  $\langle S_{\mathbf{0}}^z(0) S_{\mathbf{r}}^z(0) \rangle$ , while having qualitatively similar shape to that of (4), does not match the classical correlator  $\chi_{\text{cl}}(\mathbf{r}) = \langle n_{\mathbf{0}}^z n_{\mathbf{r}}^z \rangle$ , especially so for sites at which the sign

of the correlation changes with temperature (such as sites 3 and 7 in Fig. 3 for which the sign of  $\chi(\mathbf{r})$  changes from ferromagnetic at high  $T$  to antiferromagnetic one below  $T \approx 0.5$ ).

Mapping long-range correlations in quantum models onto the renormalized classical behavior is rather standard on approach to the ordered state [13]. What we observe is fundamentally different: quantum-to-classical correspondence, or QCC, is valid in the intermediate temperature regime at all distances, including nearest-neighbor sites, and when the correlation length  $\xi$  is still very short, of the order of the lattice spacing,  $\xi \sim 1$ . It is worth noting that this short-distance correspondence is also very different from the high- $T$  quasiclassical wave regime of Ref. 13 which allows for the classical description at distances  $r \sim \xi \gg 1$ .

We find that QCC also takes place for the  $s = 1/2$  square lattice Heisenberg antiferromagnet where, thanks to the absence of a sign problem for the path-integral Monte Carlo simulation, it has a relative accuracy of  $\sim 0.3\%$  at all temperatures (down to the ground state in a finite-size system). These facts suggest that QCC in 2D is extremely accurate and thus may take place for other lattices (however, it does not hold for 1D chains).

The quality of the matching procedure allows us to establish the  $T_{\text{cl}}(T)$  correspondence with an accuracy of about one percent. In the right panel of Fig. 3 we plot the final result along with the asymptotic high-temperature relation  $T_{\text{cl}} = (4/3)T$  reflecting the difference between the  $\langle S^z \rangle^2 = 1/4$  and  $\langle (n^z)^2 \rangle = 1/3$ . An immediate consequence of observed QCC in Fig. 3 is that the entire  $\mathbf{q}$  dependence of the static susceptibility  $\chi(\mathbf{q}, \omega_n = 0)$  of the quantum model is given by the susceptibility of the classical model at temperature  $T_{\text{cl}}(T)$ , which is readily available from classical Monte Carlo simulations.

Due to the limited low-temperature range of the  $T_{\text{cl}}(T)$  curve for the TLHA it is perhaps too early to make any definite conclusion regarding its extrapolation down to the  $T = 0$  limit. One possibility is that it smoothly extrapolates to a finite value  $T_{\text{cl}}(0) = 0.28$ , implying that the ground state is some kind of a spin liquid. This possibility was discussed by Anderson [17] almost forty years ago but was subsequently rejected on the basis of numerous investigations which include exact diagonalization [18–20], Green’s function MC calculations [21], series expansion [22], density matrix renormalization group [23] studies, as well as large- $S$  (spin wave) [24–26], large- $N$  [27], and functional renormalization group analysis [28]. Note, however, that the spin correlation length for the classical model at  $T_{\text{cl}} \approx 0.28$  is above  $10^3$  lattice periods [15] and thus simulations of small system sizes  $L \sim 10$  would be severely affected by finite-size effects. The value of  $T_{\text{cl}}(0) \approx 0.28$  is surprisingly close (essentially within the error bars) to the temperature obtained by extrapolating transition temperatures for the  $q = 3$  Potts transition in finite magnetic fields  $h$  to the  $h = 0$

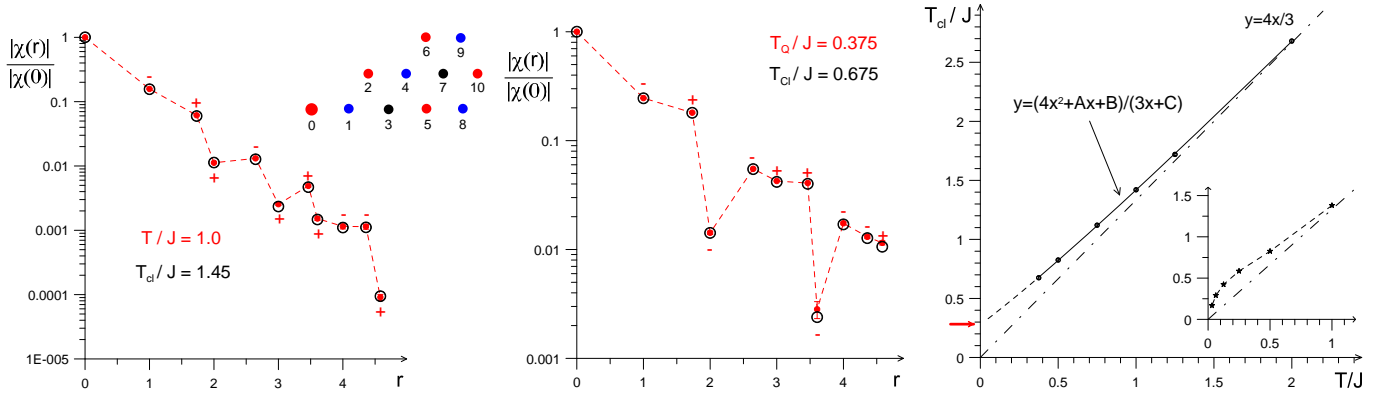


FIG. 3. (Color online) Left and middle panels: Perfect match of the normalized quantum and classical responses at the corresponding temperatures,  $T$  and  $T_{cl}(T)$ . Points are ordered according to their distance from the origin,  $r$ , as is illustrated in the right top corner. The sign of the correlator is indicated explicitly next to the point. Right Panel: Mapping between the classical and quantum temperatures. The solid (continued as dashed) line is the fitting function,  $y = (4x^2 + Ax + B)/(3x + C)$ , with  $A = 0.462$ ,  $B = 1.065$ ,  $C = 3.825$ , which satisfies the asymptotic law  $y = 4x/3$  expected in the high-temperature limit shown by the dash-dotted line. The red arrow indicates the position of the chiral transition advocated in Refs. [14–16]. For comparison, the square lattice data (stars) are shown in the inset.

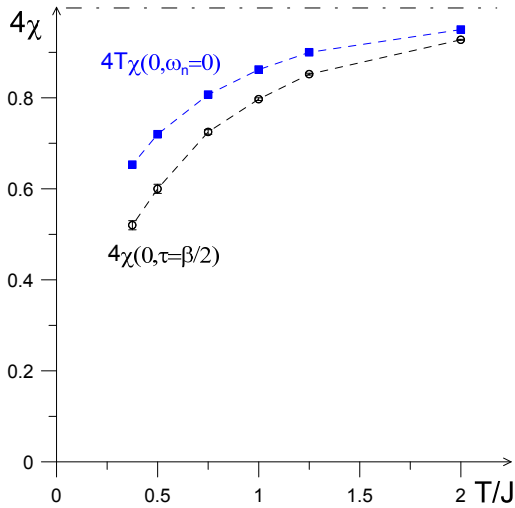


FIG. 4. (Color online) Blue (square) symbols: local static susceptibility  $\chi(r = 0, \omega_m = 0)$ , multiplied by  $4T$ , as a function of  $T/J$ . Black circles show  $T$  dependence of the (4 times) local spin correlation function  $\chi(r = 0, \tau = \beta/2)$ .

limit [29, 30]. Large-scale MC simulations performed in zero magnetic field also identify  $T_{cl} = 0.285(5)$  as the critical point of the chiral transition [14–16]. However, the debate with regards to the existence of the chiral transition is not settled yet—an alternative scenario [31, 32] predicts a sharp crossover to a more standard nonlinear sigma-model type behavior around  $T_{cl} = 0.28$ .

The other possibility is that the QCC curve  $T_{cl}(T)$  will cross over to the standard renormalized classical behavior in the long wavelength limit and will arrive at  $T_{cl}(0) = 0$ , implying the ordered quantum ground state. This is exactly what happens for the square lattice antiferromag-

net, see inset in the right panel in Fig. 3. In fact, it is also known (and can be readily deduced from the correspondence plot and Fig.2 of Ref. 15) that in the TLHA the renormalized classical regime with large correlation length emerges only below temperature  $T \approx 0.25$  [33, 34], which is well below our lowest data point  $T = 0.375$ . Clearly, more data at lower temperatures are required in order to resolve this fascinating question.

The normalization factor  $\chi(0) \equiv \chi(r = 0, \omega_m = 0)$  in Fig. 3 is given by the local static susceptibility which of course is different for the classical and quantum system. For the classical Heisenberg model  $T\chi(0)$  is simply  $1/3$ , independent of temperature, while in the quantum system this quantity is  $T$  dependent, as Fig. 4 shows. The same figure also shows the local spin correlation function at  $\tau = \beta/2$ ,  $\chi(r = 0, \tau = \beta/2) = T \sum_m e^{i\pi m} \chi(r = 0, \omega_m)$ . This too probes quantum fluctuations, i.e., contributions to the sum from terms with  $\omega_m \neq 0$ . As expected, both curves deviate from unity with the lowering of  $T$ , reflecting the increasing role of quantum fluctuations.

Perhaps the most striking feature of QCC is its predictive power in the search for spin-liquid states. Indeed, if QCC is confirmed for a given model of quantum magnetism and the classical ground state is not ordered due to macroscopic degeneracy then the quantum ground state is not ordered as well; i.e., it is a spin liquid. Moreover, even if the classical ground state is ordered but the correspondence curve  $T_{cl}(T)$  is such that  $T_{cl}(0) \neq 0$ , the quantum ground state is still not ordered similarly to its finite-temperature classical counterpart. While the final outcome for the TLHA remains to be seen, our data convincingly show an unusual classical-to-quantum correspondence with regards to the static spin correlations.

We thank M. Rigol for comments and the original NLC data and R.R.P. Singh for comments. This work was supported by the National Science Foundation under Grants No. PHY-1005543 (S.K., N.P., B.S., and C.N.V.) and No. DMR-1206774 (O.A.S.), and by a grant from the Army Research Office with funding from the DARPA.

- 
- [1] N. Prokof'ev and B. Svistunov, *Phys. Rev. Lett.* **99**, 250201 (2007).
- [2] K. Van Houcke, F. Werner, E. Kozik, N. Prokof'ev, B. Svistunov, M. J. H. Ku, A. T. Sommer, L. W. Cheuk, A. Schirotzek, and M. W. Zwierlein, *Nat. Phys.* **8**, 366 (2012).
- [3] E. Y. Loh, J. E. Gubernatis, R. T. Scalettar, S. R. White, D. J. Scalapino, and R. L. Sugar, *Phys. Rev. B* **41**, 9301 (1990).
- [4] V. N. Popov and S. A. Fedotov, *Sov. Phys. - JETP* **67**, 535 (1988).
- [5] V. N. Popov and S. A. Fedotov, *Proc. Steklov Inst. Math.* **177**, 184 (1991).
- [6] N. V. Prokof'ev and B. V. Svistunov, *Phys. Rev. B* **84**, 073102 (2011).
- [7] F. J. Dyson, *Phys. Rev.* **85**, 631 (1952).
- [8] W. Zheng, R. R. P. Singh, R. H. McKenzie, and R. Coldea, *Phys. Rev. B* **71**, 134422 (2005).
- [9] M. Rigol, T. Bryant, and R. R. P. Singh, *Phys. Rev. E* **75**, 061118 (2007).
- [10] S. Kulagin, N. Prokof'ev, O. Starykh, B. Svistunov, and C. Varney, *Phys. Rev. B* **87**, 024407 (2013).
- [11] K. Van Houcke, E. Kozik, N. Prokof'ev, and B. Svistunov, "Diagrammatic Monte Carlo," in *Computer Simulation Studies in Condensed Matter Physics XXI*, edited by D. Landau, S. Lewis, and H. Schuttler (Springer Verlag, Heidelberg, Berlin, 2008).
- [12] The number of topologically distinct diagrams within the  $G^2W$ -skeleton scheme was calculated in Ref. [35]; the eight lowest orders are 1, 1, 6, 49, 542, 7278, 113824, 2017881.
- [13] S. Sachdev, *Quantum Phase Transitions* (Cambridge University Press, Cambridge, England, 1999).
- [14] H. Kawamura and S. Miyashita, *J. Phys. Soc. Jpn.* **53**, 4138 (1984).
- [15] H. Kawamura, A. Yamamoto, and T. Okubo, *J. Phys. Soc. Jpn.* **79**, 023701 (2010).
- [16] B. Southern and H.-J. Xu, *Phys. Rev. B* **52**, R3836 (1995).
- [17] P. Anderson, *Materials Research Bulletin* **8**, 153 (1973).
- [18] B. Bernu, C. Lhuillier, and L. Pierre, *Phys. Rev. Lett.* **69**, 2590 (1992).
- [19] P. Sindzingre, P. Lecheminant, and C. Lhuillier, *Phys. Rev. B* **50**, 3108 (1994).
- [20] S. Yunoki and S. Sorella, *Phys. Rev. B* **74**, 014408 (2006).
- [21] L. Capriotti, A. E. Trumper, and S. Sorella, *Phys. Rev. Lett.* **82**, 3899 (1999).
- [22] Z. Weihong, R. H. McKenzie, and R. R. P. Singh, *Phys. Rev. B* **59**, 14367 (1999).
- [23] S. R. White and A. L. Chernyshev, *Phys. Rev. Lett.* **99**, 127004 (2007).
- [24] S. J. Miyake, *J. Phys. Soc. Jpn.* **61**, 983 (1992).
- [25] A. V. Chubukov, S. Sachdev, and T. Senthil, *J. Phys.: Cond. Mat.* **6**, 8891 (1994).
- [26] A. L. Chernyshev and M. E. Zhitomirsky, *Phys. Rev. B* **79**, 144416 (2009).
- [27] S. Sachdev, *Phys. Rev. B* **45**, 12377 (1992).
- [28] J. Reuther and R. Thomale, *Phys. Rev. B* **83**, 024402 (2011).
- [29] M. V. Gvozdikova, P.-E. Melchy, and M. E. Zhitomirsky, *J. Phys: Cond. Matt.* **23**, 164209 (2011).
- [30] L. Seabra, T. Momoi, P. Sindzingre, and N. Shannon, *Phys. Rev. B* **84**, 214418 (2011).
- [31] P. Azaria, B. Delamotte, and D. Mouhanna, *Phys. Rev. Lett.* **68**, 1762 (1992).
- [32] B. W. Southern and A. P. Young, *Phys. Rev. B* **48**, 13170 (1993).
- [33] N. Elstner, R. R. P. Singh, and A. P. Young, *Phys. Rev. Lett.* **71**, 1629 (1993).
- [34] W. Zheng, J. O. Fjærestad, R. R. P. Singh, R. H. McKenzie, and R. Coldea, *Phys. Rev. B* **74**, 224420 (2006).
- [35] L.G. Molinari and N. Manini, *Eur. Phys. J. B* **51**, 331 (2006).